J Biol Inorg Chem (2014) 19:29–44
DOI 10.1007/s00775-013-1052-y

ORIGINAL PAPER

Di- and polynuclear silver(I) saccharinate complexes of tertiary diphosphane ligands: synthesis, structures, in vitro DNA binding, and antibacterial and anticancer properties

Veysel T. Yilmaz · Elif Gocmen · Ceyda Icsel · Murat Cengiz · Sunde Y. Susluer · Orhan Buyukgungor

Received: 10 July 2013 / Accepted: 28 September 2013 / Published online: 17 October 2013

Abstract A series of new silver(I) saccharinate (sac) complexes, $[Ag_2(sac)_2(\mu\text{-dppm})H_2O]\cdot H_2O$ (**1**), $\{[Ag_2(\mu\text{-sac})_2(\mu\text{-dppe})]\cdot 3H_2O\cdot CH_2Cl_2\}_n$ (**2**), $[Ag_2(\mu\text{-sac})_2(\mu\text{-dppp})]_n$ (**3**), and $[Ag(sac)(\mu\text{-dppb})]_n$ (**4**) [dppm is 1,1-bis(diphenylphosphino)methane, dppe is 1,2-bis(diphenylphosphino) ethane, dppp is 1,3-bis(diphenylphosphino)propane, and dppb is 1,4-bis(diphenylphosphino)butane], have been synthesized and characterized by C, H, N elemental analysis, IR spectroscopy, ^{1}H NMR, ^{13}C NMR, and ^{31}P NMR spectroscopy, electrospray ionization mass spectrometry, and thermogravimetry–differential thermal analysis. Single-crystal X-ray studies show that the diphosphanes act as bridging ligands to yield a dinuclear complex (**1**) and one-dimensional coordination polymers (**2** and **4**), whereas the sac ligand adopts a μ_2-N/O bridging mode in **2**, and is N-coordinated in **1** and **4**. The interaction of the silver(I) complexes with fish sperm DNA was investigated using UV–vis spectroscopy, fluorescence spectroscopy, and agarose gel electrophoresis. The binding studies indicate that the silver(I) complexes can interact with fish sperm DNA through intercalation, and complexes **1** and **3** have the highest binding affinity. The gel electrophoresis assay further confirms the binding of the complexes with the pBR322 plasmid DNA. The minimum inhibitory concentrations of the complexes indicate that complex **1** exhibits very high antibacterial activity against standard bacterial strains of *Escherichia coli*, *Salmonella typhimurium*, and *Staphylococcus aureus*, being much higher than those of $AgNO_3$, silver sulfadiazine, ciprofloxacin, and gentamicin. Moreover, complexes **1**–**3** exhibit very high cytotoxic activity against A549 and MCF-7 cancer cell lines, compared with $AgNO_3$ and cisplatin. The bacterial and cell growth inhibitions of the silver(I) complexes are closely related to their DNA binding affinities.

Keywords Silver(I) complexes · Saccharinate · Tertiary diphosphanes · DNA binding · Antibacterial activity

V. T. Yilmaz (✉) · E. Gocmen · C. Icsel
Department of Chemistry,
Faculty of Arts and Sciences,
Uludag University,
16059 Bursa, Turkey
e-mail: vtyilmaz@uludag.edu.tr

M. Cengiz
Department of Pharmacology and Toxicology,
Faculty of Veterinary Medicine,
Uludag University,
16059 Bursa, Turkey

S. Y. Susluer
Department of Medical Biology,
Medical Faculty, Ege University,
35100 Izmir, Turkey

O. Buyukgungor
Department of Physics,
Faculty of Arts and Sciences,
Ondokuz Mayis University,
55139 Samsun, Turkey

Introduction

Elemental silver and silver(I) compounds have been used as antimicrobial agents for decades [1–4], and the antimicrobial activity depends on the release of Ag^+ ions. Silver sulfadiazine (AgSD) was introduced as an antibacterial and antifungal agent to prevent bacterial infections in cases of severe burns [5–11]. AgSD has a polymeric structure, in which the silver(I) ions are coordinated by the nitrogen atoms of the pyrimidine ring and

sulfonyl oxygen atoms of sulfadiazine molecules [12, 13]. Its effectiveness as an antimicrobial agent is due to its tendency to dissociate in solution, providing a steady supply of silver(I) ions over a period of time [6]. The mechanism for the antimicrobial action of silver(I) ions is not properly understood; however, it is generally accepted that they interfere with cell growth in three ways: (1) inhibition of transport functions in the cell wall, (2) interruption of cell metabolism, and (3) interaction with DNA [14–16]. Moreover, it was concluded that the magnitude of antimicrobial properties of silver complexes is related to the ease with which they participate in ligand exchange reactions [17]. The biological activity of silver(I) complexes with oxygen-donor ligands comes from the weaker bonding property of the Ag–O bonds. In the biological system, the ease of ligand replacement of the silver(I) complexes will result in further replacement with biological ligands as protein, enzymes, and membrane-containing thiol groups in their active sites [18–21].

The water-soluble alkali salts of saccharin (also named 1,1-dioxo-1,2-benzothiazol-3-one or *o*-benzosulfimide) are widely used as a noncaloric artificial sweetener and food additive. The imino hydrogen of saccharin is acidic and thus in solution the molecule can be easily converted into the corresponding nitranion, saccharinate (sac). Sac has different coordination sites, such as one negatively charged imino nitrogen atom, one carbonyl oxygen atom, and two sulfonyl oxygen atoms. As a polyfunctional ligand, it is able to form metal complexes from mononuclear to coordination polymers, but in the case of bulky ligands, it sometimes remains outside the coordination sphere as a counterion [22]. Although a large number of metal complexes of sac have been reported in the literature, their biological activities have received less attention and only a few metal complexes of sac with anticancer activity have been reported. For example, $K[Pt(sac)_3(H_2O)]$ and [(PTA)Au(sac)] (PTA is 1,3,5-triaza-7-phosphaadamantane) exhibited strong antigrowth effects on HeLa and A2780 cells, respectively [23, 24]. We recently reported a number of highly cytotoxic palladium(II) and platinum(II) complexes of sac with bis(2-pyridylmethyl)amine [25], 2,2′:6′,2″-terpyridine [26–28], 2-(hydroxymethyl)pyridine [29], and 2-(2-hydroxyethyl)pyridine [29]. The DNA binding studies indicated that the metal sac complexes with 2,2′:6′,2″-terpyridine interact with fish sperm DNA (FS-DNA) strongly via both intercalation and coordination as dual-function metallointercalators [30].

In addition to their antimicrobial properties, the anticancer activities of silver(I) complexes have received great attention in the last decade. The main advantage of the use of silver(I) complexes in the development of new anticancer drugs is their low toxicity toward humans [31]. Recently, Banti and Hadjikakou [32] reviewed the antiproliferative and antitumor properties of silver(I) compounds. The literature shows that in some cases, silver(I) complexes exhibit significant anticancer activity compared with cisplatin, a clinically used anticancer drug.

The synthesis and structures of silver(I) sac complexes with phosphine ligands were not studied extensively, and there is only one example, $[Ag(sac)(PPh_3)_2]$ [33]. In addition, to the best of our knowledge, there is as yet little information available concerning biological evaluation of silver(I) complexes of sac, and only two studies of their antimicrobial activities have been reported [34, 35]. It was found that $[Ag(sac)]_n$ was very effective on a wide range of bacteria [35]. The encouraging results with regard to the antibacterial and anticancer activities of the metal complexes of sac led us to design a series of new silver(I) complexes bearing both sac and diphosphine ligands (named as phosphane by IUPAC), namely, $[Ag_2(sac)_2(\mu\text{-dppm})H_2O]\cdot H_2O$ (**1**), $\{[Ag_2(\mu\text{-sac})_2(\mu\text{-dppe})]\cdot 3H_2O\cdot CH_2Cl_2\}_n$ (**2**), $[Ag_2(\mu\text{-sac})_2(\mu\text{-dppp})]_n$ (**3**), and $[Ag(sac)(\mu\text{-dppb})]_n$ (**4**) [dppm is 1,1-bis(diphenylphosphino)methane, dppe is 1,2-bis(diphenylphosphino)ethane, dppp is 1,3-bis(diphenylphosphino)propane, and dppb is1,4-bis(diphenylphosphino)butane] (Fig. 1)]. The interactions of these complexes with DNA were studied using absorption and fluorescence spectroscopy, and gel electrophoresis measurements. Furthermore, in vitro antibacterial activity tests were performed on Gram-negative and Gram-positive bacteria, and in vitro anticancer activities were tested against two human cancer

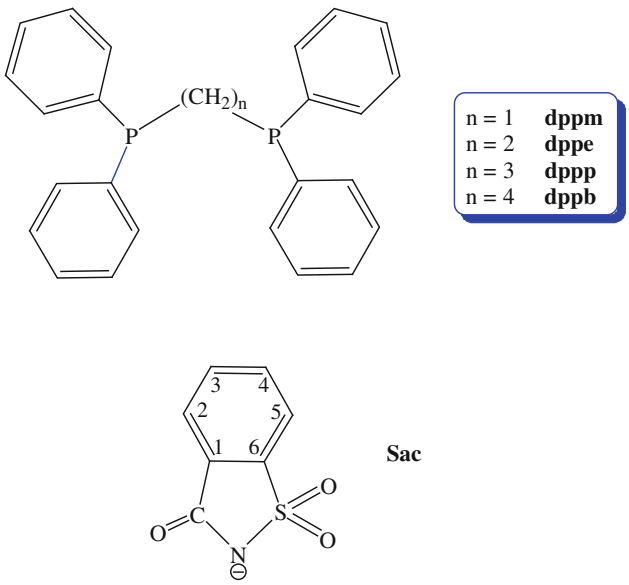

Fig. 1 Tertiary diphosphane and saccharinate (*sac*) ligands used in the synthesis of $[Ag_2(sac)_2(\mu\text{-dppm})H_2O]\cdot H_2O$ (**1**), $\{[Ag_2(\mu\text{-sac})_2(\mu\text{-dppe})]\cdot 3H_2O\cdot CH_2Cl_2\}_n$ (**2**), $[Ag_2(\mu\text{-sac})_2(\mu\text{-dppp})]_n$ (**3**), and $[Ag(sac)(\mu\text{-dppb})]_n$ (**4**), and the numbering scheme for NMR spectroscopy

cell lines (A549 and MCF-7) as well as a normal cell line (WI-38).

Materials and methods

All chemicals used in the experiments were commercial products and were used without further purification. Elemental analyses for carbon, hydrogen, and nitrogen were performed using a Costech elemental analyzer. UV–vis spectra were measured with a PerkinElmer Lambda 35 spectrophotometer. IR spectra were recorded from 400 to 4,000 cm^{-1} with a Thermo Nicolet 6700 Fourier transform (FT) IR spectrophotometer and are reported with the following abbreviations: vs (very strong), s (strong), m (medium), w (weak), and vw (very weak). ^{1}H NMR and ^{13}C NMR spectra were recorded with a Varian Mercuryplus spectrometer at 400 and 100 MHz, respectively, in dimethyl-d_6 sulfoxide (DMSO-d_6) using tetramethylsilane as an internal reference at room temperature, whereas ^{31}P NMR spectra were recorded with an INOVA-500 spectrometer at 200 MHz in DMSO-d_6. Thermal analysis curves [thermogravimetry (TG) and differential thermal analysis (DTA)] were obtained using a Seiko Exstar TG/DTA 6200 thermal analyzer in a flowing air atmosphere with a heating rate of 10 °C min^{-1} using a sample size of 5–10 mg and platinum crucibles. Fluorescence spectra were recorded at room temperature with a Varian Cary Eclipse spectrophotometer equipped with a xenon pulse lamp of 75 kW. For all fluorescence measurements, both slits were maintained at 5 nm. The electrospray ionization (ESI) mass spectra were recorded using a Bruker Daltonics micrOTOF II ESI time-of-flight mass spectrometer. The electrical conductivity measurements of MeOH and DMSO solutions of the silver(I) complexes were performed with an Inolab Cond 730 conductimeter at room temperature and are reported as Λ_M (S cm^2 mol^{-1}).

Synthesis of **1**

A solution of Na(sac)·$2H_2O$ (0.06 g, 0.25 mmol) in MeCN/MeOH (10 mL, 1:1) was added dropwise to a solution of $AgNO_3$ (0.04 g, 0.25 mmol) in MeOH (5 mL) and the mixture was stirred for 30 min at room temperature. Then, dppm (0.05 g, 0.125 mmol) in MeCN (5 mL) was added to the solution. The resulting clear solution was stirred for 2 h and allowed to stand in darkness at room temperature. Colorless crystals were formed after 3 days. Yield 0.180 g, 72 %. Melting point 256–272 °C (decomp.). Anal. Calcd for $C_{39}H_{34}Ag_2N_2O_8P_2S_2$ (%): C, 46.80; H, 3.43; N, 2.80. Found (%): C, 46.84; H, 3.61; N, 2.83. ^{1}H-NMR (400 MHz, DMSO-d_6, δ, ppm): 7.87–7.55 (m, 28H, Ph-sac and Ph-dppm), 2.05 (s, 2H, CH_2-dppm). ^{13}C NMR (100 MHz, DMSO-d_6, δ, ppm): 168.33 (C=O-sac), 144.19 (C6-sac), 133.72 (d, C_{ipso}-P), 133.27 (d, C4-sac), 133.12 (C3-sac), 132.89 (C1-sac), 132.05 (Ph-C_{ortho}-P), 131.21 (Ph-C_{para}-P), 129.06d (Ph-C_{meta}-P), 123.83 (C2-sac), 120.46 (C5-sac). ^{31}P NMR (200 MHz, DMSO-d_6, δ, ppm): 8.82 [t, $^{1}J(^{31}P\text{-}Ag)$ = 504, 688 Hz]. FT-IR (KBr, cm^{-1}): 3,044 (w) $\nu(C_{arom}\text{-}H)$], 2,913 (w), 2,844 (vw) $\nu(C_{alf}\text{-}H)$, 1,639 (vs) $\nu(C{=}O)$, 1,332 (m) $\nu_s(CNS)$, 1,291 (vs), 1,258 (s) $\nu_{as}(SO_2)$, 1,153 (vs) $\nu_s(SO_2)$, 1,111 (s), 960 (s) $\nu_{as}(CNS)$, 754 (s), 691 (m) $\nu(C\text{–}P)$, 679 (m), 601 (s), 510 (m). ESI^+ mass spectrometry (MS) (MeOH) *m*/*z*: 491.0 $[Ag(dppm)]^+$, 634.9 $[Ag_2(sac)(MeOH)Na]^+$, 781.9 $[Ag_2(sac)(dppm)]^+$, 1,019.0 $[Ag_2(dppm)_2Cl]^+$, 1,166.0 $[Ag_2(sac)(dppm)_2]^+$, 1,309.9 $[Ag_3(sac)_3(dppm)(MeOH)Na]^+$, 1,547.0 $[Ag_2(sac)(dppm)_3]$. Λ_M (MeOH, 25 °C, 10^{-3} M) 58 S cm^2 mol^{-1}. Λ_M (DMSO, 25 °C, 10^{-3} M) 14 S cm^2 mol^{-1}.

Synthesis of **2**

Na(sac)·$2H_2O$ (0.06 g, 0.25 mmol) in water (5 mL) was added to a solution of $AgNO_3$ (0.04 g, 0.25 mmol) in water (5 mL). The solution immediately became milky. The addition of MeCN (10 mL) to the milky suspension resulted in a clear solution. The addition of dppe (0.05 g, 0.125 mmol) in CH_2Cl_2 (5 mL) to the solution resulted in a biphasic solution, which turned into a monophasic clear solution on addition of a mixture of DMSO and MeCN (10 mL, 2:1). The resulting solution was allowed to stand in darkness at room temperature. A colorless polycrystalline powder precipitated within 4 days. Yield 0.096 g, 70 %. Melting point 276–285 °C (decomp.). Anal. Calcd for $C_{41}H_{40}Ag_2Cl_2N_2O_9P_2S_2$ (%): C, 44.10; H, 3.61; N, 2.50. Found (%): C, 44.61; H, 3.89; N, 2.44. ^{1}H-NMR (400 MHz, DMSO-d_6, δ, ppm): 7.95–7.36 (m, 28H, Ph-sac and Ph-dppe), 5.77 (s, 2H, CH_2Cl_2), 2.57 (s, 4H, CH_2-dppe). ^{13}C NMR (100 MHz, DMSO-d_6, δ, ppm): 167.54 (C=O-sac), 144.17 (C6-sac), 133.38 (d, C_{ipso}-P), 133.19 (C4-sac), 133.03 (C3-sac), 132.31 (d, Ph-C_{ortho}-P), 132.02 (Ph-C_{para}-P), 131.34 (C1-sac), 129.49 (d, Ph-C_{meta}-P), 123.80 (C2-sac), 120.42 (C5-sac), 55.37 (C-CH_2Cl_2). ^{31}P NMR (200 MHz, DMSO-d_6, δ, ppm): 10.04 [d, $^{1}J(^{31}P\text{-}Ag)$ = 579 Hz]. FT-IR (KBr, cm^{-1}): 3,085 (w), 3,056 (w), 3,015 (vw) $\nu(C_{arom}\text{-}H)$, 2,909 (w), 2,852 (vw) $\nu(C_{alf}\text{-}H)$, 1,655 (vs) $\nu(C{=}O)$, 1,332 (m) $\nu_s(CNS)$, 1,279 (vs), 1,246 (vs) $\nu_{as}(SO_2)$, 1,140 (vs) $\nu_s(SO_2)$, 1,111 (s), 960 (vs) $\nu_{as}(CNS)$, 747 (s), 731 (s), 690 (s) $\nu(C\text{–}P)$, 669 (s), 600 (s), 510 (m). ESI^+–MS (MeOH) *m*/*z*: 461.1 $[Ag_2(sac)(MeOH)_2]^+$, 507.0 $[Ag(dppe)]^+$, 706.0 $[Ag_3(sac)_2(H_2O)]^+$, 752.0 $[Ag_3(sac)_2(MeOH)_2]^+$, 795.9 $[Ag_2(sac)(dppe)]^+$, 859.2 $[Ag_2(sac)(dppe)(MeOH)_2]^+$, 905.2 $[Ag(dppe)_2]^+$. Λ_M (MeOH, 25 °C, 10^{-3} M) 29 S cm^2 mol^{-1}. Λ_M (DMSO, 25 °C, 10^{-3} M) 9 S cm^2 mol^{-1}.

Synthesis of **3**

To a solution of $AgNO_3$ (0.04 g, 0.25 mmol) in MeOH (5 mL), Na(sac)·$2H_2O$ (0.06 g, 0.25 mmol) in MeOH/MeCN (10 mL, 1:1) was added. After 30 min stirring at room temperature, the addition of dppp (0.052 g, 0.125 mmol) in MeCN (5 mL) resulted in the formation of a clear solution. The evaporation of the solution at room temperature gave a white powder. The powder was washed with water and dried at room temperature. Yield 0.099 g, 80 %. Melting point 230–235 °C. Anal. Calcd for $C_{41}H_{34}Ag_2N_2O_6P_2S_2$ (%): C, 43.13; H, 3.14; N, 2.82. Found (%): C, 43.00; H, 2.50; N, 2.88. ^{1}H-NMR (400 MHz, DMSO-d_6, δ, ppm): 7.86–7.36 (m, 28H, Ph-sac and Ph-dppp), 2.62 (q, 4H, CH_2-dppp), 2.05 (s, 2H, CH_2-dppp). ^{13}C NMR (100 MHz, DMSO-d_6, δ, ppm): 167.23 (C=O-sac), 143.88 (C6-sac), 133.43 (d, C_{ipso}-P), 133.19 (Ph-C_{ortho}-P), 132.79 (C4-sac), 132.50 (C3-sac), 132.19 (d, C1-sac), 131.21 (Ph-C_{para}-P), 129.43 (d, Ph-C_{meta}-P), 123.85 (C2-sac), 120.45 (C5-sac). ^{31}P NMR (200 MHz, DMSO-d_6, δ, ppm): 5.86 (sbr). FT-IR (KBr, cm^{-1}): 3,074 (vw), 3,055 (w), 3,010 (vw) ν(C_{arom}-H), 2,921 (vw), 2,864 (vw) ν(C_{alf}-H), 1,635 (s) ν(C=O), 1,329 (m) ν_s(CNS), 1,283 (vs), 1,251 (s) ν_{as}(SO_2), 1,148 (vs) ν_s(SO_2), 1,119 (s), 953 (s) ν_{as}(CNS), 744 (s), 693 (s) ν(C–P), 677 (vs), 597 (vs), 513 (s). ESI$^+$–MS (MeOH) *m/z*: 519.0 $[Ag(dppp)]^+$, 809.9 $[Ag_2(sac)(dppp)]^+$, 933.2 $[Ag(dppp)_2]^+$, 1,014.9 $[Ag_2(sac)_2(dppp)Na]^+$, 1,222.1 $[Ag_2(sac)(dppp)_2]^+$, 1,365.9 $[Ag(dppp)_3(H_2O)]^+$. Λ_M (MeOH, 25 °C, 10^{-3} M) 21 S cm^2 mol^{-1}. Λ_M (DMSO, 25 °C, 10^{-3} M) 11 S cm^2 mol^{-1}.

Synthesis of **4**

Complex **4** was prepared by the same procedure as described for **2** with Na(sac)·$2H_2O$ (0.03 g, 0.125 mmol) and dppb (0.054 g, 0.125 mmol). Colorless crystals were formed after 2 days. Yield 0.070 g, 78 %. Melting point 279–287 °C (decomp.). Anal. Calcd for $C_{35}H_{32}AgNO_3P_2S$ (%): C, 58.70; H, 4.50; N, 1.95. Found (%): C, 59.22; H, 4.79; N, 1.99. ^{1}H-NMR (400 MHz, DMSO-d_6, δ, ppm): 7.84–7.38 (m, 24H, Ph-sac and Ph-dppb), 2.36 (s, 4H, CH_2-dppb), 1.55 (s, 4H, CH_2-dppb). ^{13}C NMR (100 MHz, DMSO-d_6, δ, ppm): 167.60 (C=O-sac), 144.14 (C6-sac), 133.39 (d, C_{ipso}-P), 133.15 (C4-sac), 133.03 (C3-sac), 132.99 (d, C1-sac), 132.75 (Ph-C_{ortho}-P), 131.14 (Ph-C_{para}-P), 129.44 (d, Ph-C_{meta}-P), 123.75 (C2-sac), 120.36 (C5-sac). ^{31}P NMR (200 MHz, DMSO-d_6, δ, ppm): 5.86 [d, $^1J(^{31}P$-Ag) = 488 Hz]. FT-IR (KBr, cm^{-1}): 3,065 (w), 3,007 (vw) ν(C_{arom}-H), 2,926 (w), 2,897 (w), 2,856 (vw) ν(C_{alf}-H), 1,643 (s) ν(C=O), 1,328 (m) ν_s(CNS), 1,281 (vs), 1,254 (m) ν_{as}(SO_2), 1,151 (vs) ν_s(SO_2), 1,115 (s), 957 (s) ν_{as}(CNS), 744 (s), 695 (s) ν(C–P), 600 (m), 514 (m). ESI$^+$–MS (MeOH) *m/z*_ 535.1 $[Ag(dppb)]^+$, 677.0 $[Ag_2Cl(dppb)]^+$, 824.0 $[Ag_2(sac)(dppb)]^+$, 1,103.1 $[Ag_2Cl(dppb)_2]^+$, 1,250.2 $[Ag_2(sac)(dppb)_2]^+$, 1,394.1 $[Ag_3Cl(sac)(dppb)]^+$, 1,535.9 $[Ag_3(sac)_2(dppb)_2]^+$. Λ_M (MeOH, 25 °C, 10^{-3} M) 46 S cm^2 mol^{-1}. Λ_M (DMSO, 25 °C, 10^{-3} M) 14 S cm^2 mol^{-1}.

X-ray crystallography

The intensity data for complexes **1**, **2**, and **4** were collected with an STOE IPDS 2 diffractometer with graphite-monochromatized Mo K_α radiation ($\lambda = 0.71073$ Å) at 296 (2) °C. The structures were solved by direct methods and refined on F^2 with the SHELX-97 program [36]. All non-hydrogen atoms were found from the difference Fourier map and were refined anisotropically, whereas the hydrogen atoms bound to carbons were refined using a riding model, but those of water were refined freely. Compounds **1** and **2** contain highly disordered water molecules, which were eliminated from the refinement of these structures by means of the SQUEEZE subroutine of PLATON [37], and the *hkl* intensities were modified accordingly. In addition, the crystal of **2** was a nonmerohedral twin (twin lattice quasi-symmetry) crystal with two reciprocal lattices differently oriented, giving rise to double diffraction spot sets. The data sets of the twin parts for two different crystals were integrated separately and then scaled to give the *hkl* set used. But, because the partial overlapped reflections could not be integrated separately, the reflection count and reflection angle are less than 85 and 65 %, respectively. Crystal data and refinement details are summarized in Table 1.

Crystallographic data (without structure factors) for the structures reported in this article have been deposited with the Cambridge Crystallographic Data Centre (CCDC) as supplementary publication no. CCDC 949365–949367. Copies of the data can be obtained free of charge from the CCDC via http://www.ccdc.cam.ac.uk/data_request/cif.

DNA binding studies

The concentrations of the complexes in various solutions used in this work were based on their empirical formula. FS-DNA solutions of various concentrations (0–100 μM) dissolved in a tris(hydroxymethyl)aminomethan (Tris)–HCl buffer (pH 7) were added to complexes **1**–**4** (10 μM dissolved in MeOH). The amount of MeOH in these final solutions was 4.0 %. The values of *r* (ratio of complex concentration to DNA concentration) ranged from 0.1 to 1.0. Absorption spectra were recorded after equilibrium had been attained at 20 °C for 10 min. The intrinsic binding constant (K_b) was determined using the following equation [38]:

$$[DNA]/(\varepsilon_a - \varepsilon_f) = [DNA]/(\varepsilon_b - \varepsilon_f) + 1/K_b(\varepsilon_b - \varepsilon_f) \quad (1)$$

where [DNA] is the concentration of DNA in base pairs, ε_a, ε_f, and ε_b correspond to A_{obs}/[M], the extinction coefficient

Table 1 Crystallographic data and structure refinement for complexes **1**, **2**, and **4**

	1	**2**	**4**
Empirical formula	$C_{39}H_{32}Ag_2N_2O_7P_2S_2$	$C_{20}H_{16}AgNO_3PS$	$C_{35}H_{32}AgNO_3P_2S$
Formula weight	982.47	489.25	716.49
Crystal system	Monoclinic	Triclinic	Monoclinic
Space group	$P2_1/c$	$P^{-}1$	$P2_1/c$
a (Å)	12.297 (2)	8.6916 (15)	20.3361 (4)
b (Å)	15.466 (2)	11.293 (4)	14.9758 (3)
c (Å)	21.449 (4)	11.632 (2)	27.2484 (6)
α (°)	90	91.36 (2)	90
β (°)	96.204 (15)	106.884 (15)	126.417 (1)
γ (°)	90	102.57(2)	90
V (Å^3)	4,055.6 (12)	1,061.7 (4)	6,677.9 (2)
Z	4	2	8
ρ_{calcd} (g cm^{-3})	1.609	1.530	1.425
μ (mm^{-1})	1.197	1.141	0.797
$F(000)$	1,968	490	2,928
θ (°)	1.6–26.5	1.8–26.0	1.2–26.5
Collected reflections	37,270	8,285	99,408
Data/restraints/parameters	8,424/4/493	2,706/6/244	13,833/0/755
Goodness of fit on F^2	1.01	0.89	0.97
R_1 ($I > 2\sigma$)	0.065	0.060	0.041
wR_2	0.110	0.108	0.086

See Fig. 1 for the structures of the complexes

of the free metal(II) complex, and the extinction coefficient of the complex in the fully bound form, respectively. The ratio of the slope to the intercept in the plot of [DNA]/($\varepsilon_a - \varepsilon_f$) versus [DNA] gives the value of K_b.

Ethidium bromide (EB)–FS-DNA fluorescence quenching experiments were conducted in the buffer by keeping the ratio of the DNA concentration to the EB concentration at 10 (50 μM DNA, 5 μM EB), and then the silver(I) complexes (2.5–50 μM) in MeOH were added to this solution. The buffer used in the binding studies was 20 mM Tris–HCl (pH 7.0), containing 20 mM NaCl. All solutions were allowed to equilibrate thermally at 20 °C for about 30 min before measurements. The fluorescence spectra of the solutions were recorded in the range from 500 to 750 nm with an excitation wavelength of 295 nm. The quenching ability of the complexes was evaluated by the Stern–Volmer constant (K_{SV}) [39]:

$$I_0/I = 1 + K_{SV}\,[\text{complex}] \tag{2}$$

where I_0 and I are the emission intensities in the absence and presence of the complexes, respectively. K_{SV} depends on the ratio of the concentration of bound EB to the concentration of DNA and is also called the quenching constant. On the other hand, the binding constants K_{app} and K_A were determined from Eq. 3 [40] and Eq. 4 [41], respectively:

$$K_{EB}[\text{EB}] = K_{app}\,[\text{complex}] \tag{3}$$

in which the complex concentration is that which results in a 50 % reduction of the fluorescence intensity of EB and $K_{EB} = 1.0 \times 10^7\ \text{M}^{-1}$ (5.0 μM EB);

$$\log(F_0 - F)/F = n\log K_A - n\log\{\ 1/[\text{complex}] - [\text{EB} - \text{DNA}](F_0 - F)/F_0\} \tag{4}$$

where [EB−DNA] and [complex] are the total concentration of EB−DNA and silver(I) complexes, respectively. The plot of $\log(F_0 - F)/F$ versus $\log\{1/([\text{complex}] - [\text{EB}-\text{DNA}](F_0 - F)/F_0)\}$ was drawn and fitted linearly, and then the slope gives n, which is the number of binding sites per nucleotide.

The interaction of the silver(I) complexes with supercoiled pBR322 plasmid DNA was monitored using agarose gel electrophoresis. The plasmid DNA (10 μM) in Tris–HCl/EDTA buffer (pH 7.6) was treated with different amounts of the silver(I) complexes (10–100 μM) in MeOH, followed by dilution with the Tris–HCl buffer to a total volume of 10 μL. Then, the samples were incubated at 37 °C for 1.5 h. A dye solution, containing 0.05 % bromophenol blue, 40 % sucrose, 0.5 % sodium lauryl sulfate,

and 0.1 M EDTA, was added to the reaction mixture prior to electrophoresis. Then, the samples were electrophoresed on 1 % agarose gel with 1 μg/mL EB, using 0.5× Tris–borate–EDTA buffer (pH 8.0) for 1 h at 120 V at room temperature. Finally, the gel was photographed under UV light.

Antibacterial activity

Bacterial strains of *Escherichia coli* (ATCC 25922 and O157:H7), *Salmonella typhimurium* (ATCC 14028), and *Staphylococcus aureus* (ATCC 25923 and ATCC 33591) were used.

Broth microdilution testing was performed to determine the minimum inhibitory concentrations (MICs) of ciprofloxacin, gentamicin, and the silver(I) complexes according to the guidelines of the Clinical Laboratory Standards Institute [42]. The bacterial cultures were prepared in Mueller–Hinton broth at 37 °C for 20 h. All compounds were dissolved in DMSO. Freshly prepared stock solutions were sterilized using 0.20-μm single-use filter units (Minisart, Sartorius Stedim Biotech). Dilutions ranging from 0.007 to 775 μM were prepared in Mueller–Hinton broth, and inocula with a density equivalent to 0.5 McFarland turbidity were added to tubes containing the dilutions of the compounds. After incubation at 37 °C for 20 h, the MICs were defined as the minimum concentration of the compound that inhibited growth of the organism. The optical densities of the cultures were measured at a wavelength of 595 nm (iMark, Bio-Rad). All MIC determinations were performed in duplicate.

Cytotoxic activity

The samples for in vitro tests were obtained from 50 mM stock solutions of the complexes in neat DMSO. The stock solutions were then sequentially diluted with the required amount of cell culture medium in order to obtain the solutions studied, the concentration of which ranged from 1 nM to 100 μM. Untreated cells were used as a control group (0.2 % DMSO vehicle).

WST-1 viability assay (4-[3-(4-iodophenyl)-2-(4-nitrophenyl)-2*H*-5-tetrazolio]-1,3-benzene disulfonate sodium salt, Roche Applied Science) was performed to examine the cytotoxic effects of the concentrations of complexes **1**–**4** that cause 50 % inhibition of cells (IC_{50}) on A549 (human lung carcinoma), MCF-7 (human breast adenocarcinoma), and WI-38 (normal human fibroblasts) cell lines. The assay is based on the cleavage of the tetrazolium salt by viable cells into a colored formazan product that can be measured spectrophotometrically. For this purpose, these cell lines were incubated at a density of 1×10^4 cells per milliliter using 96-well plates for 24, 48, and 72 h. After the incubation periods, 10 μL of WST-1 solution was added to each well, followed by incubation at 37 °C for 1 h. The absorbance (optical density) of each well was read at wavelengths of 450 and 630 nm using a microplate reader (Multiskan FC, Thermo Scientific). Each compound was tested at every concentration in triplicate in a single experiment, which was repeated three times. $AgNO_3$ and cisplatin were used as reference cytotoxic agents. Values obtained for the vehicle-treated cells were used as the reference for 100 % viability. IC_{50} values were determined by sigmoidal dose–response functions using GraphPad Prism.

Results and discussion

Synthesis and characterization

The complexes were synthesized by the reaction of $Na(sac)\cdot 2H_2O$ with $AgNO_3$ in the presence of the equivalent amount of the tertiary diphosphanes in solution at room temperature. The analytical data confirmed the stoichiometry of complexes **1**–**4**. The structures of complexes **1**, **2**, and **4** were confirmed by X-ray crystallography. Complex **1** has a dinuclear structure, whereas complexes **2** and **4** are coordination polymers. In some cases, the molecular formula differs as a result of recrystallization. For example, the polycrystalline powder of **2** has three water molecules and a CH_2Cl_2 solvate in the empirical formula, but it contains only a water molecule in the crystal form, as will be discussed below. Regrettably our attempts to grow X-ray-quality crystals of complex **3** failed; however, on the basis of elemental analysis, IR spectroscopy, and NMR spectroscopy, complex **3** is assumed to have a molecular structure similar to that of complex **2**, but it does not contain any solvent molecules such as water or CH_2Cl_2 present in **2**. All complexes were obtained in high yields (over 70 %). Complexes **1**–**3** are stable to light for a long time, but complex **4** begins to turn brown after 2 weeks. On the other hand, the solutions of the complexes in MeOH and DMSO were kept for up to 72 h at room temperature and were checked by ^1H and ^{13}C NMR spectroscopy. The observations showed that these solutions did not change color during that time and also that there was no decomposition product in the NMR spectra. Moreover, a comparison of the initial ^1H and ^{13}C NMR spectra of the solutions of the silver(I) complexes with those after 72 h indicated that the spectra were identical and the chemical shifts (δ) differ by only 0.03 ppm for the ^1H NMR spectra and 2.0 ppm for the ^{13}C NMR spectra. All the complexes are nonhygroscopic and highly soluble in MeOH, MeCN, and DMSO. The electrical conductivity measurements indicate that the complexes exhibit a nonelectrolytic

behavior, with Λ_M ranging from 21 to 58 S cm^2 mol^{-1} in MeOH, and from 9 to 14 S cm^2 mol^{-1} in DMSO [43].

The thermal stability of the silver(I) complexes was studied by TG–DTA. Complex **1** dehydrates between 57 and 157 °C with a mass loss of 3.0 % (calculated 2.9 %), involving the lost of both the lattice and coordination water molecules. Then, the anhydrite complex begins to decompose exothermically at around 260 °C, and the decomposition ends at approximately 580 °C. The total mass loss of 76.7 % is consistent with the formation of Ag_2O (the calculated mass value is 77.8 %). The mass loss up to 86 °C is due to the removal of the CH_2Cl_2 solvate in **2**, followed by dehydration. The complex decomposes exothermically between 270 and 700 °C to give Ag_2O (total mass loss, found 80.1 % and calculated 79.3 %). Complexes **3** and **4** are stable up to approximately 300 °C, and their decompositions end at around 800 °C. The mass losses are in accord with the structures of these complexes and suggest the formation of Ag_2O as the final decomposition product.

Complexes **1**–**4** were characterized by the positive-ion ESI–MS spectra. The different cationic species present in MeOH solution of the complexes were identified, and most relevant data are reported in "Materials and methods." The isotopic distribution of these species is consistent with the calculated composition. The strongest peaks for these complexes usually correspond to dinuclear silver(I) species such as $[Ag_2(sac)(dppm)_3]^+$, $[Ag_2(sac)(dppp)_2]^+$, and $[Ag_2(sac)(dppb)_2]^+$ in accordance with possible aggregation in solution and formation of these species. However, in the case of **2**, the $[Ag(dppe)_2]^+$ cation is the most abundant. In addition, the ESI–MS spectra also exhibit several less intense peaks related to the presence of mononuclear $[Ag(diphos)]^+$ or $[Ag(diphos)_2]^+$ and dinuclear $[Ag_2(sac)]^+$ cations, arising from fragmentation under the conditions used [44–49].

The spectral characterizations were performed using polycrystalline powders of the silver(I) complexes. In the IR spectra of complexes **1**–**4**, the bands between 2,852 and 3,085 cm^{-1} are due to the absorption of the phenyl and CH_2 groups. The C=O vibration of the sac ligand is observed as a very sharp band at in the frequency range from 1,635 to 1,655 cm^{-1}. The asymmetric stretching of the SO_2 group appears to be split into two strong bands at approximately 1,280 and 1,250 cm^{-1}, whereas the symmetric stretching is observed as a sharp band at approximately 1,150 cm^{-1}. A 10-cm^{-1} decrease in $\nu_s(SO_2)$ in the spectrum of **2** is evidence for the coordination via the sulfonyl group in this complex. The bands at 1,425–1,450 and 1,000 cm^{-1} are usually assigned to the P–C vibrations of the free forms of the phosphane ligands [50, 51]. However, in the case of mixed-ligand metal complexes, it is very difficult to assign these bands, and therefore the very strong absorption bands centered at around 690 cm^{-1} were attributed the P–C bonds in the free forms of the ligands and their complexes [52].

The ^{1}H, ^{13}C, and ^{31}P NMR spectra of complexes **1**–**4** were measured at room temperature in DMSO-d_6 solution. The aromatic protons of both sac and diphosphanes appear

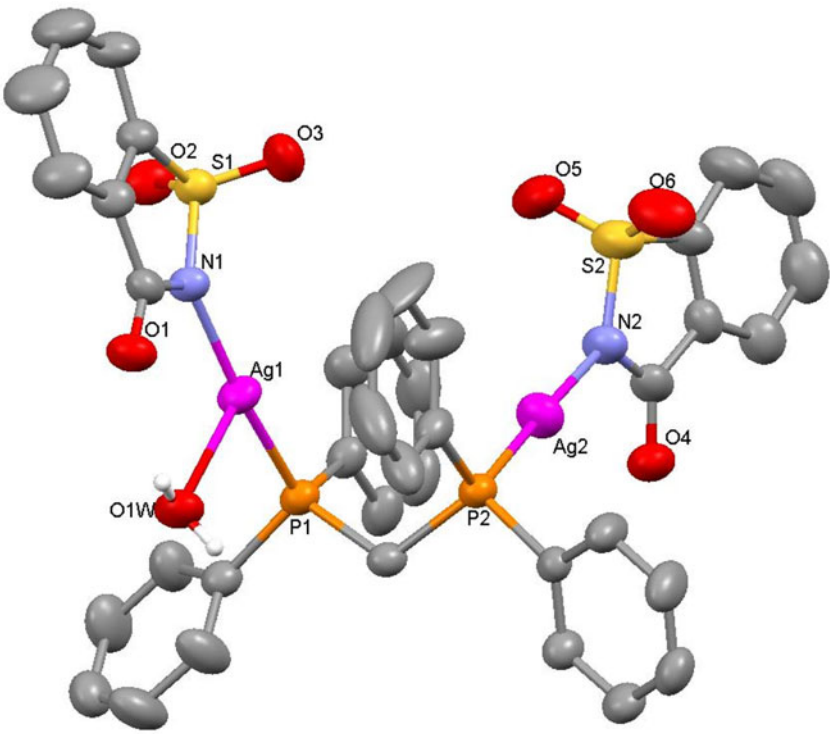

Fig. 2 Molecular structure of **1**. All C–H hydrogen atoms are omitted for clarity. The probability level of thermal ellipsoids is 40 %

between 7.36 and 7.95 ppm as multiplets. The bridging methylene protons in **1** and **2** are observed as a singlet at 2.05 and 2.57 ppm, respectively, whereas those in **3** and **4** are centered at 2.05–2.62 and 1.55–2.36 ppm, respectively, as doublets. The methylene protons of the diphosphanes generally experience deshielding on complexation. In addition, there was a detectable signal at δ 5.77 ppm corresponding to the protons of the CH_2Cl_2 solvate in **2**. In the ^{13}C NMR spectra of the complexes, the carbonyl group of the sac ligand occurs at approximately δ 167.50 ppm, whereas the chemical shifts for the phenyl carbons are observed in the range from 120.0 to 144.0 ppm. The ^{31}P NMR spectra of complexes of silver(I) with phosphorous-donor ligands usually exhibit splitting owing to the ^{1}J(P-Ag) coupling. The phosphorous nuclei in the diphosphane ligands experience deshielding by approximately 22.0–32.0 ppm at room temperature compared with those in the free forms of the ligands. The ^{31}P NMR spectrum of complex **1** consists of a triplet centered at 8.82 ppm with two coupling constants of 504 and 688 Hz. These different

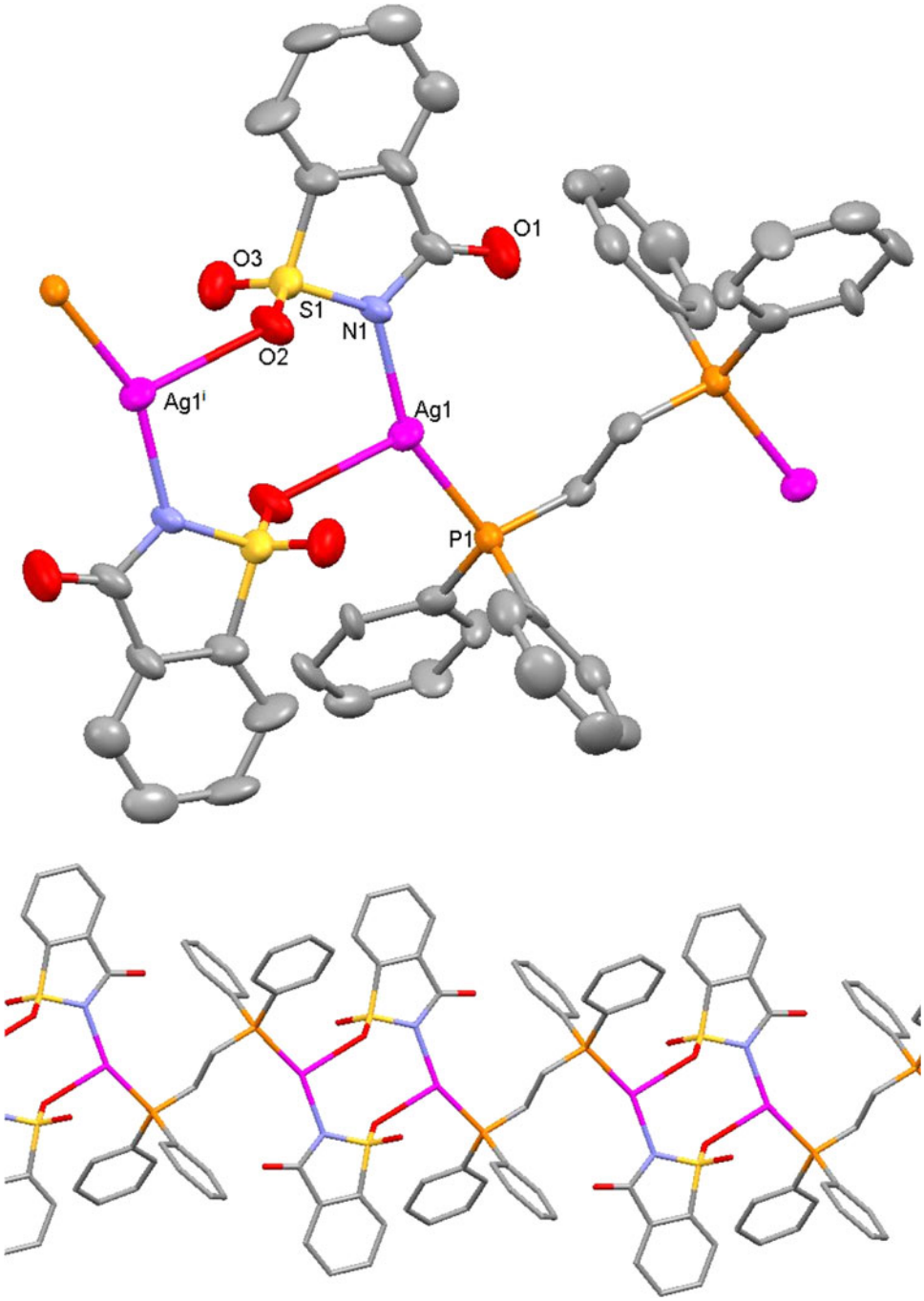

Fig. 3 The coordination environment around silver(I) and the one-dimensional polymeric structure of **2**. Hydrogen atoms were omitted for clarity. The probability level of thermal ellipsoids is 40 %. Symmetry code: $-x + 1, -y + 1, -z + 1$

coupling constants are believed to arise from the different chemical environments around the phosphorous nuclei in **1**, as will be shown in the X-ray structure of the complex. On the other hand, the spectra of **2** and **4** reveal well-resolved doublets at 10.04 and 5.86 ppm, respectively. The calculated coupling constants of $^{1}J(^{31}\text{P}\text{-}^{107,109}\text{Ag})$ are 579 Hz for **2** and 488 Hz for **4**, being typical of silver(I) complexes containing the corresponding diphosphane ligands [47, 48]. In particular, the ^{31}P NMR spectrum of **3** consists of a broad singlet at 5.86 ppm, presumably in consequence of reasonably fast exchange equilibrium at room temperature.

Description of crystal structures

The molecular structures of complexes **1**, **2** and **4** together with their numbering schemes are given in Figs. 2, 3, and 4. Selected bond lengths and angles are given in Table 2. The diphosphanes in these silver(I) complexes behave as bridging ligands as expected [53, 54], whereas the sac ligand exhibits different coordination modes [22]. Complex **1** has a dinuclear structure, in which the dppm ligand bridges the two silver(I) centers. In addition, each silver(I) ion is coordinated by a nitrogen-donor sac ligand. These two silver(I) ions exhibit different coordination geometry: one has a linear geometry with an angle of 175.49 (17)°, whereas the other one displays a T-shaped geometry with the additional coordination of an aqua ligand (Fig. 2). The Ag–N bond distances of 2.151 (5) and 2.132 (5) Å are typical for silver(I) complexes containing a nitrogen-bonded sac ligand [35, 55–66], whereas both Ag–P bond distances are identical, being 2.3550 (17) Å and similar to those found in the silver(I) complexes of dppm [67–74], but significantly shorter than the corresponding bonds in silver(I) complexes containing the same ligand [44–46, 49, 72, 75–96]. These short Ag–P bond distances in complex **1** may be due to the low coordination number

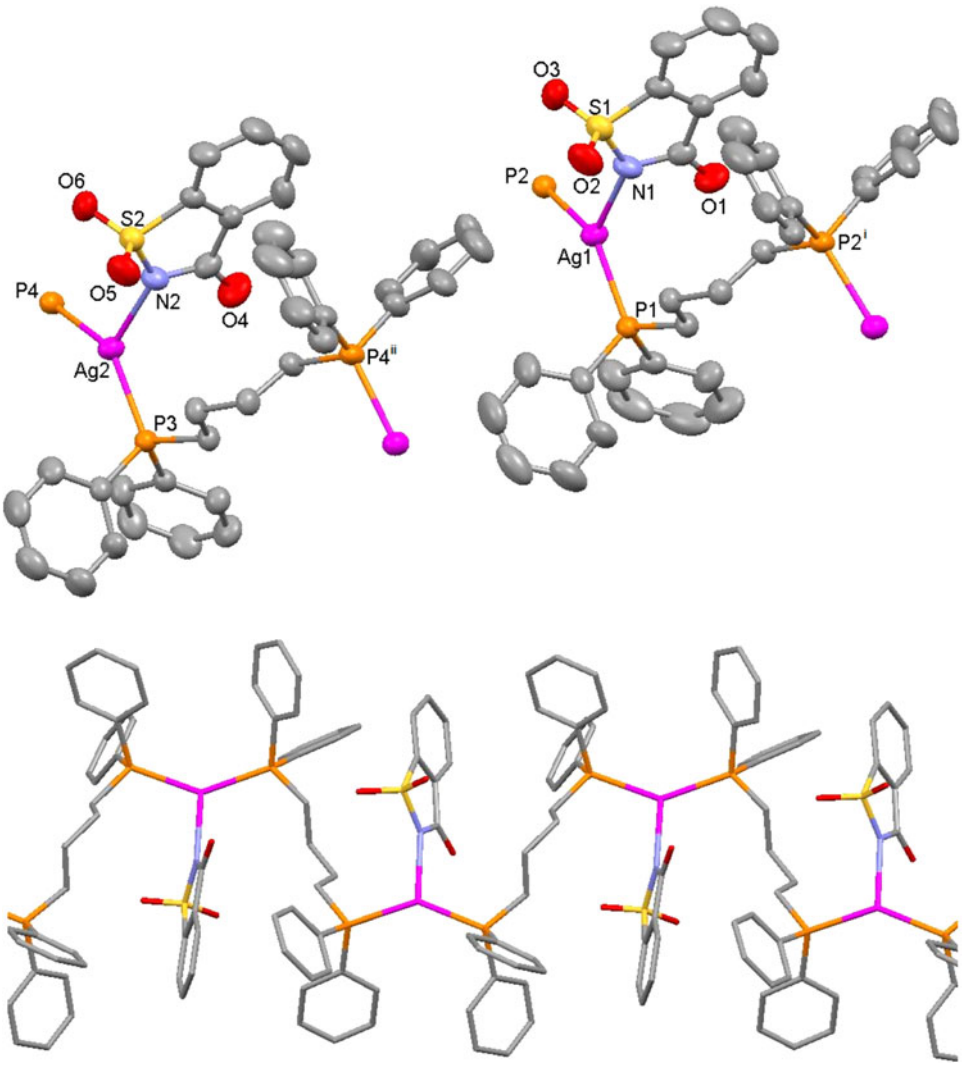

Fig. 4 View of the coordination environment around silver(I) and the one-dimensional polymeric structure of **4**. Hydrogen atoms were omitted for clarity. The probability level of thermal ellipsoids is 40 %. Symmetry codes: (*i*) $-x + 2$, $y + 1/2$, $-z + 3/2$; (*ii*) $-x + 1$, $y + 1/2$, $-z + 1/2$

Table 2 Selected bond lengths (Å) and angles (°) for complexes **1**, **2**, and **4**

	1	2	4
Ag1–N1	2.151 (5)	2.160 (8)	2.313 (2)
Ag2–N2	2.132 (5)	–	2.336 (2)
Ag1–P1	2.3550 (17)	2.356 (3)	2.4115 (8)
Ag1–P2	2.3552 (17)	–	2.4198 (8)
Ag2–P3	–	–	2.4212 (8)
Ag2–P4	–	–	2.4300 (8)
Ag1–O1W	2.594 (4)	–	–
Ag1–O2^{i}	–	2.527 (7)	–
N1–Ag1–P1	169.11 (13)	156.0 (2)	112.70 (7)
N1–Ag1–P2	–	–	106.67 (7)
N2–Ag1–P2	175.49 (17)	–	–
N1–Ag1–O1W	95.27 (16)	–	–
N1–Ag1–O2^{i}	–	95.6 (3)	–
P1–Ag1–O1W	95.40 (12)	–	–
P1–Ag1–P2	–	–	140.17 (3)
N2–Ag2–P3	–	–	112.39 (7)
N2–Ag2–P4	–	–	107.54 (7)
P3–Ag2–P4	–	–	139.59 (3)
P1–Ag1–O2^{i}	–	108.37 (18)	–

Symmetry code: $-x+1,-y+1,-z+1$

of silver(I) and relatively less steric hindrance of the sac ligand compared with the co-ligands in the other silver(I) complexes of dppm. The individual molecules of **1** are connected by strong intermolecular O–H···O hydrogen bonds between the aqua and sac ligands in the adjacent species. Moreover, relatively weak interactions such as C–H···O [C···O bond distance 3.464 (8) to 3.485 (7) Å] and π(sac)···π(sac) [$C_g\cdots C_g$ bond distance 3.811 Å (x, $-1+y$, z); C_g, ring centroid] are also present in **1**.

Complex **2** is a one-dimensional coordination polymer of $\{[Ag_2(\mu\text{-sac})_2(\mu\text{-dppe})]\cdot H_2O\}_n$. The sac ligands adopt a μ_2-bridging mode via the imino nitrogen and the sulfonyl oxygen atoms, forming dinuclear $[Ag(sac)]_2$ units with a chairlike eight-membered ring. The coordination geometry around each silver(I) ion is T-shaped. The $[Ag_2(sac)_2]$ units are further bridged by the dppe ligands, leading to a linear polymeric chain of **2** (Fig. 3). The Ag–N and Ag–O bond distances are 2.160 (8) and 2.527 (7) Å, respectively, and are in the range of those reported for silver(I) complexes containing $N,O_{sulfonyl}$ bridging sac ligands [56, 97–99]. The Ag–P bond distance in complex **2** is 2.356 (3) Å (Table 2), being similar to the bond distances found in the silver(I) complexes of dppe reported in [70, 100], but it is obviously shorter than the bond distances for silver(I) complexes of dppe reported in [44, 47, 49, 91, 101–

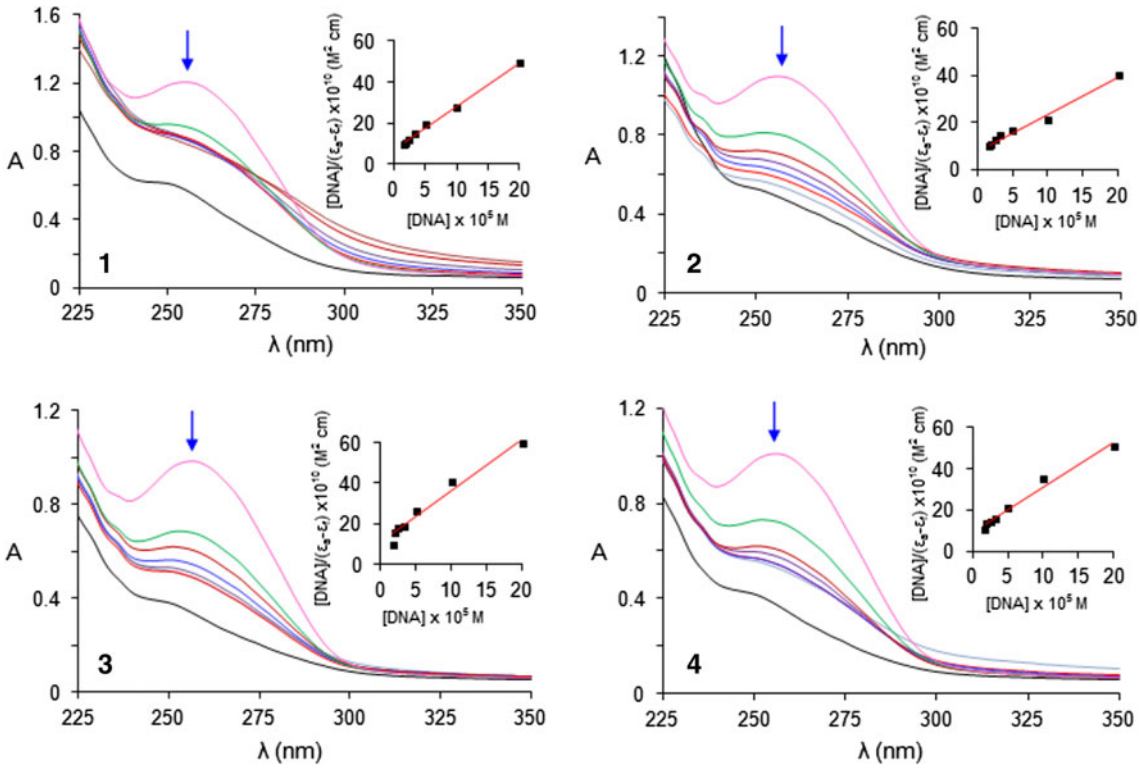

Fig. 5 UV–vis spectra of complexes **1**–**4** (10 μM) in MeOH solution in the presence of increasing amounts of fish sperm DNA (0–100 μM). The *arrows* show the changes in absorbance with increasing amounts of fish sperm DNA. *Insets* [DNA]/($\varepsilon_a - \varepsilon_f$) versus [DNA]

110]. As mentioned earlier, the complex contains a highly disordered water molecule, which was removed during the refinement. The presence of the lattice water molecule is important for hydrogen bonding between the chains in **2**, but the exclusion of the water molecule makes the discussion of the crystal packing meaningless. However, it can be said that in addition to the possible hydrogen-bonding interactions involving the water molecules, the chains are connected by π(sac)$\cdots\pi$(sac) stacking interactions of 3.65 (1) Å (symmetry code $1 - x, -y, 1 - z$) and the structure of **2** is further reinforced by C–H$\cdots\pi$(dppe) and C–H$\cdots$O interactions, ranging from 3.00 (3) to 3.28 (2) Å.

As shown in Fig. 4, complex **4** has two species in its asymmetric unit with a similar conformation. The structure of **4** consists of polymeric chains of $[Ag(sac)(\mu\text{-dppb})]_n$, which are built up from the bridging of the silver(I) ions by the dppb ligands (Fig. 4). The trigonal geometry around silver(I) is completed by the coordination of the sac ligand via the nitrogen atom. Although the synthesis of **4** is similar to that of **2**, it has a different polymeric structure in which the bridging of sac is probably avoided by the dppb ligand containing a much longer ethylene chain than those of dppe in **2**. The Ag–N bond distances in Table 2 are similar to those of previously reported silver(I) complexes of sac [55–66]. On the other hand, the Ag–P bond distances are in the range from 2.4115 (8) to 2.4300 (8) Å, and are similar to those found in silver(I) complexes of dppb reported in [48, 49, 110, 111], but are noticeably longer than the corresponding bonds in silver(I) complexes containing dppb reported in [70, 112]. In addition, a few examples of silver(I) complexes of dppb with much longer Ag–P bond distances have also been reported [47, 84]. The polymeric chains of **4** are connected with each other by a number of weak C–H$\cdots$O [C$\cdots$O bond distance 3.32 (2) to 3.38 (3) Å], and C–H$\cdots\pi$ [H$\cdots C_g$ bon distance 2.67 (2) to 2.96 (2) Å] interactions in the solid state.

DNA binding

Electronic absorption titration is one of the commonest methods to investigate the interactions between metal complexes and DNA. The intense absorption band centered at approximately 260 nm was used to monitor the interaction of the silver(I) complexes with FS-DNA. The electronic absorption spectra of complexes **1**–**4** in the absence and presence of increasing amounts of FS-DNA are shown in Fig. 5. The absorption band of DNA decreases in intensity with increasing DNA concentration. This is a typical "hypochromic effect," suggesting that the complexes most likely bind to DNA through intercalation. The hypochromicity of complexes **1**–**4** is 33.3, 23.5, 32.1, and 28.8 %, respectively, at $r = 0.3$. The intrinsic binding constants (K_b) of the complexes determined from Eq. 1 are given in Table 3 and Fig. 5. The K_b values are in the range from 2.00×10^4 to 3.00×10^4 M^{-1} and suggest a significant association of these complexes with FS-DNA. Complexes **1** and **3** exhibit the highest binding affinity; however, the binding constants are much lower than that reported for the classic intercalator EB ($K_b = 1.4 \times 10^6$ M^{-1}) [113].

To further clarify the nature of the binding interactions between the silver(I) complexes and DNA, competitive binding experiments were performed. The studies involved the addition of the complexes to solutions of DNA pretreated with EB, and then the measurement of the emission intensities of EB in the range from 600 to 620 nm. Fluorescence quenching of the EB–DNA complex in the presence of a new molecule can be used to realize the binding mode of the molecule. The emission spectra of EB binding to FS-DNA in the absence and presence of complexes **1**–**4** are shown in Fig. 6. A reduction in the fluorescence intensity is observed on the addition of the complexes to FS-DNA pretreated with EB. From the Stern–Volmer plots in Fig. 6, the quenching constants (K_{SV}) of the complexes were calculated (Table 3). The K_{SV} values indicate that complexes **1** and **4** exhibit greater quenching efficiency than

Table 3 Quenching constant (K_{SV}) and binding constants (K_{app} and K_A) for binding of complexes **1**–**4** and other compounds with fish sperm DNA

Compounds	K_{SV} ($\times 10^4$ M^{-1})	K_{app} ($\times 10^6$ M^{-1})	K_A ($\times 10^4$ M^{-1})	Number of binding sites per nucleotide	K_b ($\times 10^4$ M^{-1})
1	1.85 ± 0.13	1.00	1.02 ± 0.24	1.01	2.86 ± 0.16
2	0.63 ± 0.14	–[a]	0.07 ± 0.02	1.40	2.50 ± 0.22
3	0.87 ± 0.13	–[a]	0.76 ± 0.06	1.04	3.00 ± 0.12
4	1.07 ± 0.21	–[a]	0.04 ± 0.02	1.47	2.00 ± 0.17
$AgNO_3$	0.46 ± 0.01	–[a]	0.10 ± 0.07	1.20	0.83 ± 0.07
AgSD	1.97 ± 0.25	0.57	1.40 ± 0.22	1.02	3.75 ± 0.21

AgSD silver sulfadiazine

[a] These values could not be determined because the corresponding compounds did not cause a 50 % reduction in the fluorescence intensity of the ethidium bromide–DNA solutions

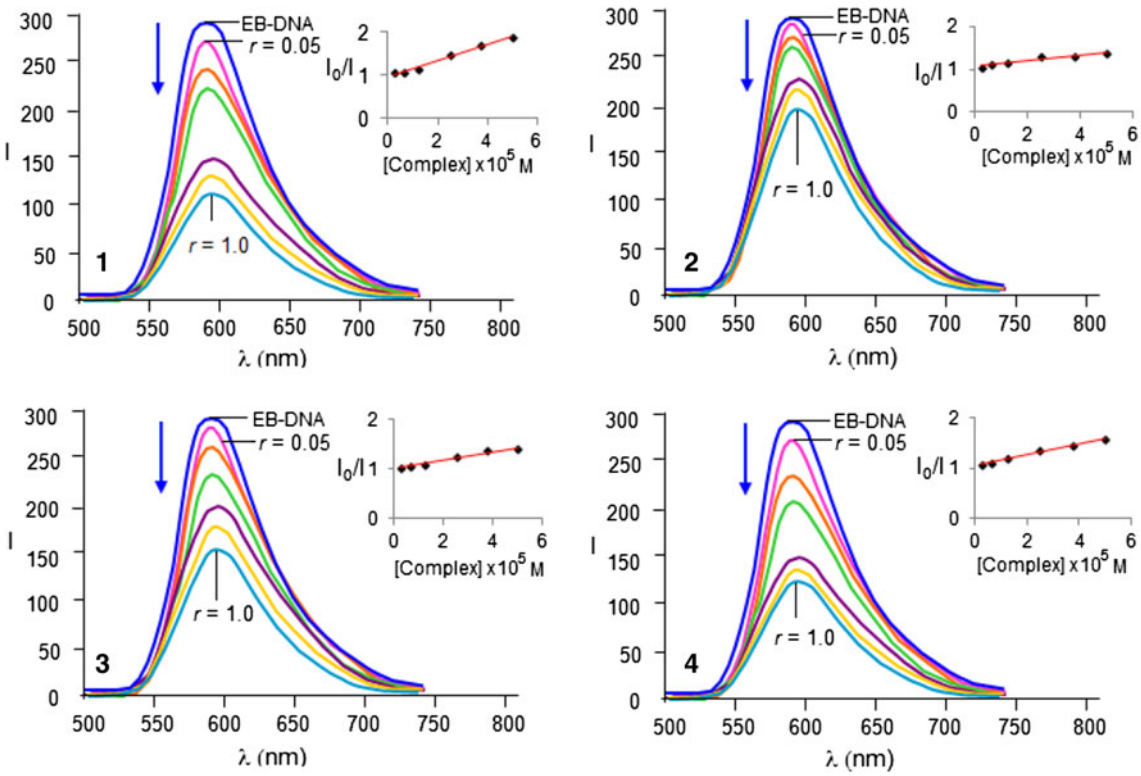

Fig. 6 Fluorescence spectra of ethidium bromide (*EB*)–DNA in the presence of increasing amounts of complexes **1**–**4** (5.0 μM EB, 50.0 μM DNA). The *arrows* show the changes in intensity on increasing amounts of the complexes. The ratio of the complex concentration to the DNA concentration is *r*. *Insets* Stern–Volmer plot of the fluorescence data

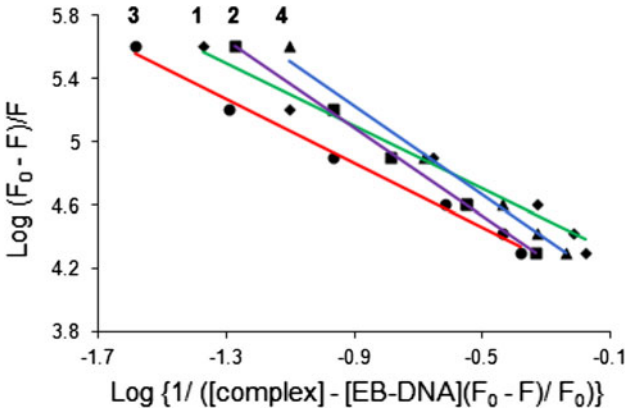

Fig. 7 Fluorescence quenching plots obtained from Eq. 4, giving the binding constants (K_A) and the number of binding sites (n) for complexes **1**–**4**

the other complexes. The DNA binding constants (K_{app} and K_A) are listed in Table 3, and the corresponding plots obtained from the experimental quenching data are shown in Fig. 7. K_{app} is the apparent binding constant and is based on the concentration of the complex that causes a 50 % reduction of the fluorescence intensity of the EB–DNA adduct (Eq. 3), and K_A is the intrinsic binding constant obtained from the fluorescence quenching studies using Eq. 4. The K_{app} values of complexes **2**–**4** and $AgNO_3$ could not be determined, because increasing their concentrations did not cause a 50 % reduction in the fluorescence intensity of the EB–DNA solutions. The interaction of complexes **1** and **3** results in the highest binding constants (K_A), and this observation is consistent with the findings (K_b) obtained from the absorption studies, suggesting that complexes **1** and **3** strongly bind to FS-DNA by an intercalative mode. However, all binding constants for AgSD were higher than those for the silver(I) complexes.

When a molecule binds to DNA it affects the size or shape of the DNA, and it will affect the electrophoretic mobility of DNA. The electrophoretic patterns of pBR322 plasmid DNA incubated with complexes **1**–**4** at various concentrations are shown in Fig. 8. The double-stranded plasmid pBR322 exists in a compact supercoiled conformation (form I), which has faster mobility compared with its closed circular (form II) and linear (form III) forms, resulting from the cleavage of one or two of the strands of the double helix. As shown in Fig. 8, complexes **2** and **4** do not have any impact on DNA mobility at the concentrations investigated, whereas complexes **1** and **3** exhibit noticeable retardation of the supercoiled DNA band with increasing complex concentration, indicating unwinding of the plasmid DNA owing to the binding of these complexes, since an intercalator is expected to unwind the DNA by lengthening and stiffening it [114].

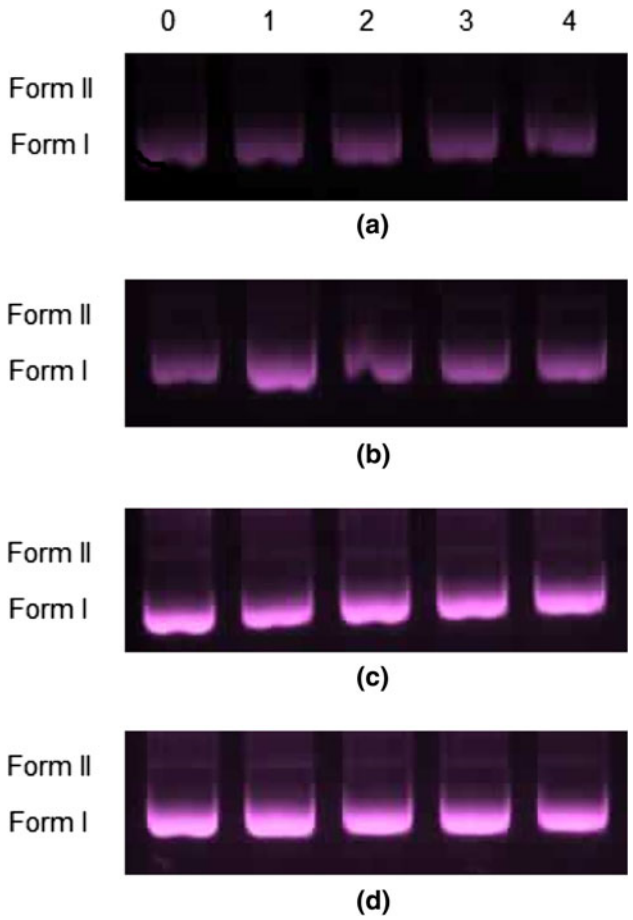

Fig. 8 Electrophoretic mobility of pBR322 plasmid DNA (10 μM) in the absence of the silver(I) complexes (*lane 0*) and in the presence of the silver(I) complexes (*a* **1**, *b* **2**, *c* **3**, and *d* **4**) at 10, 20, 50,and 100 μM (*lanes 1–4*)

Antibacterial activity

The antibacterial activities of complexes **1–4**, AgSD, $AgNO_3$, and some licensed antimicrobials against various bacterial strains are given in Table 4, as estimated by the MIC. $AgNO_3$ and AgSD were used as reference silver(I) compounds for susceptibility testing. Three bacterial species were used in this study. Among the bacterial species, *E. coli* (O157:H7) and methicillin-resistant *S. aureus* (ATCC 33591) are considered to be two of the most virulent microorganisms for the human population. The effect of the solvent (DMSO) on bacterial growth was tested and was found to be negligible. Complex **4** is totally inactive, whereas the MICs of complexes **1–3** range from 15.9 to 116.4 μM. The highest antibacterial activity is observed for complex **1** against all bacterial strains, except for *E. coli* (ATCC 25922), compared with $AgNO_3$ and AgSD (Table 4). Moreover, complex **3** also exhibits better activity against *S. typhimurium* and *S. aureus* than the antimicrobial agents and $AgNO_3$, but it has less activity than AgSD and $AgNO_3$ in the case of *E. coli*. On the other hand, complex **2** exhibits higher activity against *S. typhimurium* and *S. aureus* than the antimicrobials. The relatively high bacterial growth inhibition of these complexes is consistent with their DNA binding affinities. Although silver(I) complexes with Ag–P bonds generally exhibit weak antibacterial activity [74, 115, 116], complex **1** may be a candidate for clinical applications after further tests.

Cytotoxic activity

We tested the in vitro cytotoxic activity of complexes **1–4** against two human cancer cell lines (A549 and MCF-7) and a normal cell line (WI-38). The IC_{50} values were determined from the dose dependence of surviving cells after exposure to the silver(I) complexes for 24, 48, and 72 h (Fig. 9). The inhibition of cell proliferation by the complexes after 72 h is presented in Table 5 and is compared with inhibition by $AgNO_3$ and the clinically used anticancer agent cisplatin. The antigrowth effect of the complexes increases with increasing incubation time (Fig. 9). As shown in Table 5, the IC_{50} values of these complexes range from 0.74 to 86.40 μM and indicate that complexes **1** and **3** exhibit very high cytotoxic activity

Table 4 Antibacterial activities (minimum inhibitory concentration, μM) of complexes **1–4** and other compounds

	Escherichia coli (ATCC 25922)	*Escherichia coli* (O157:H7)	*Salmonella typhimurium* (ATCC 14028)	*Staphylococcus aureus* (ATCC 25923)	*Staphylococcus aureus* (ATCC 33591)
1	15.9	15.9	31.9	15.9	15.9
2	116.4	116.4	58.2	58.2	58.2
3	32.3	32.3	32.3	32.3	32.3
4	≥1,000	≥1,000	≥1,000	≥1,000	≥1,000
$AgNO_3$	23.5	23.5	47.1	94.2	94.2
AgSD	22.4	22.4	44.8	22.4	22.4
Ciprofloxacin	0.05	96.6	772.6	772.6	772.6
Gentamicin	33.5	134.0	536.0	134.0	134.0

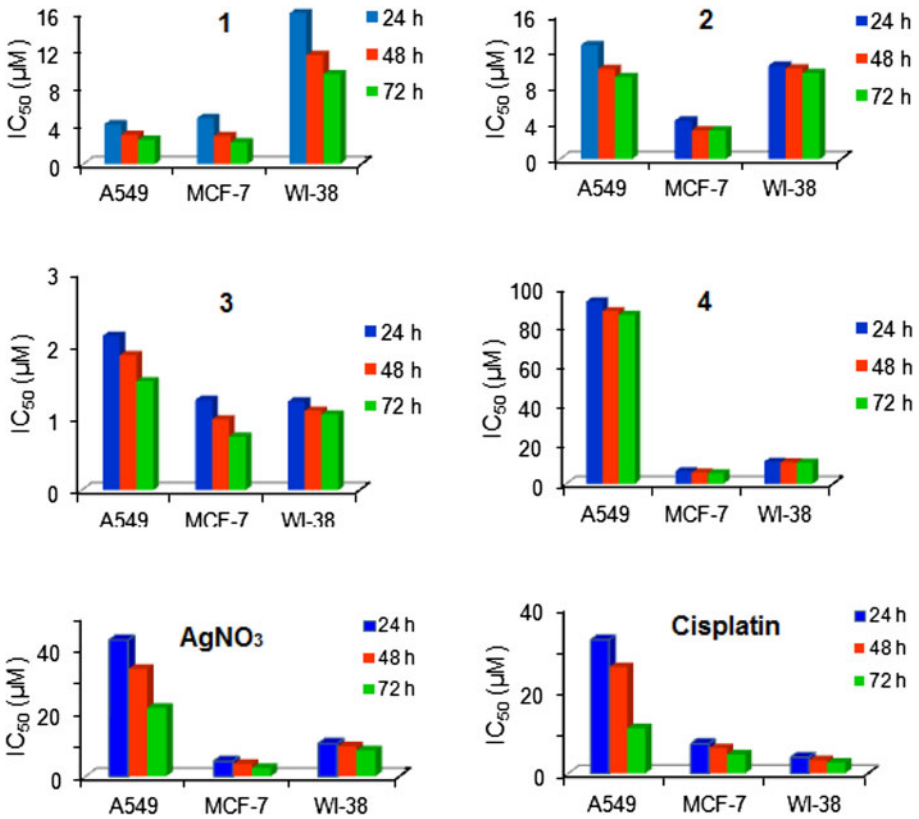

Fig. 9 The antigrowth effect of complexes **1–4**, $AgNO_3$, and cisplatin on A549, MCF-7, and WI-38 cells treated with the compounds for 24, 48, and 72 h. IC_{50} concentration that causes 50 % inhibition of cells

Table 5 Cytotoxic activities (half-maximal inhibitory concentration, μM) of silver(I) complexes **1–4**, $AgNO_3$, and cisplatin after 72 h incubation

	A549	MCF-7	WI-38
1	2.58 ± 0.83	2.32 ± 1.00	9.54 ± 2.40
2	9.11 ± 2.32	3.18 ± 1.01	2.61 ± 1.16
3	1.51 ± 0.57	0.74 ± 0.24	1.05 ± 0.53
4	86.4 ± 4.75	5.30 ± 1.61	10.78 ± 2.22
$AgNO_3$	21.51 ± 3.63	2.62 ± 1.44	8.14 ± 1.88
Cisplatin	10.92 ± 1.81	4.58 ± 1.25	2.62 ± 1.04

against all the cell lines, compared with $AgNO_3$ and cisplatin. The high inhibition activity of these complexes is in accord with their relatively high propensity to bind DNA. Among the silver(I) complexes, complex **4** is the least active against the A549 cell line, whereas its antigrowth effect on MCF-7 cells is close to that of cisplatin. The IC_{50} values of cancer and control cell lines were found to be similar. Cytotoxicity in the WI-38 cell line was evaluated as untoward side effects. Only one report on the anticancer activity of cationic silver(I) complexes with diphosphane ligands, namely, $[Ag(R_2P(CH_2)_nPR_2)_2]NO_3$ (R is Ph or Et and $n = 2$), has appeared in the literature [117] and significantly low IC_{50} values were reported for B16 melanoma cells. The anticancer activity of silver(I) complexes containing phosphane ligands has received less attention so far. The results of the present study indicate that further studies are warranted to assess their pharmacological properties and elucidate the actual mechanism of their biological activity.

Conclusion

Four new silver(I) complexes, $[Ag_2(sac)_2(\mu\text{-dppm})H_2O]\cdot H_2O$ (**1**), $\{[Ag_2(\mu\text{-sac})_2(\mu\text{-dppe})]\cdot 3H_2O\cdot CH_2Cl_2\}_n$ (**2**), $[Ag_2(\mu\text{-sac})_2(\mu\text{-dppp})]_n$ (**3**), and $[Ag(sac)(\mu\text{-dppb})]_n$ (**4**), have been synthesized and fully characterized. The structures of complexes **1**, **2**, and **4** were determined by X-ray diffraction. All phosphane ligands act as bridging ligands. The DNA binding affinity of the complexes was studied by spectroscopic methods such as absorption and fluorescence titrations. The results show that the complexes bind to DNA by intercalation. The binding of the complexes to the pBR322 plasmid DNA was further confirmed by gel electrophoresis measurements. The biological activities of the silver(I) complexes were tested against five bacterial strains and two human cancer cell lines. Among the complexes, complex **1** exhibits powerful antibacterial activity against the licensed antimicrobials, being much more powerful than $AgNO_3$ and AgSD. The cytotoxicity studies indicate that complexes **1** and **3** are very effective against

the human lung and breast cancer cell lines, and their IC_{50} values are much smaller than those of $AgNO_3$ and cisplatin. It may be concluded that the high antibacterial and anticancer activities of the silver(I) complexes correlate well with their DNA binding affinities.

Acknowledgments Financial support received from Uludag University [project UAP(F)-2011/36] is gratefully acknowledged.

References

1. Clement JL, Jarrett PS (1994) Met Based Drugs 1:467–482
2. Wright JB, Lam K, Hansen D, Burrell RE (1999) Am J Infect Control 27:344–350
3. Silver S (2003) FEMS Microbiol Rev 27:341–353
4. Klasen HJ (2000) Burns 26:117–130
5. Fox CL (1968) Arch Surg 96:184–188
6. Fox CL, Modak SM (1974) Antimicrob Agents Chemother 5:582–588
7. Fox CL (1983) Surg Gynecol Obstet 157:82–88
8. Fox CL (1985) Burns Incl Therm Inj 11:306–307
9. Deshpande LM, Chopade BA (1994) Biometals 7:49–56
10. de Gracia GG (2001) Burns 27:67–74
11. White RJ, Cooper R (2005) Wounds UK 1:51–61
12. Cook DS, Turner MF (1975) J Chem Soc Perkin Trans 2 1021–1025
13. Baenziger NC, Struss AW (1976) Inorg Chem 15:1807–1809
14. Thurman R, Gerba CP (1988) Crit Rev Environ Control 18:295–315
15. McDonnell G, Russell AD (1999) Clin Microbiol Rev 12:147–179
16. Percival SL, Bowler PG, Russell D (2005) J Hosp Infect 60:1–7
17. Kasuga NC, Yoshikawa R, Sakai Y, Nomiya K (2012) Inorg Chem 51:1640–1647
18. Liau SY, Read DC, Pugh WJ, Furr JR, Russel AD (1997) Lett Appl Microbiol 25:279–283
19. Nomiya K, Noguchi R, Oda M (2000) Inorg Chim Acta 298:24–32
20. Nomiya K, Noguchi R, Shigeta T, Kondoh Y, Tsuda K, Ohsawa K, Kasuga NC, Oda M (2000) Bull Chem Soc Jpn 3:1143–1152
21. Nomiya K, Yokohama H (2002) J Chem Soc Dalton Trans 2483–2490
22. Baran EJ, Yilmaz VT (2006) Coord Chem Rev 250:1980–1999
23. Cavicchioli M, Massabni AC, Castellano EE, Sabeh LPB, Costa-Neto CM (2007) Inorg Chim Acta 360:3055–3060
24. Maiore L, Cinellu MA, Michelucci E, Moneti G, Nobili S, Landini I, Mini E, Guerri A, Gabbiani C, Messori L (2011) J Inorg Biochem 105:348–355
25. Guney E, Yilmaz VT, Ari F, Buyukgungor O, Ulukaya E (2011) Polyhedron 30:114–122
26. Ulukaya E, Ari F, Dimas K, Sarimahmut M, Guney E, Sakellaridis N, Yilmaz VT (2011) J Cancer Res Clin Oncol 137:1425–1434
27. Ulukaya E, Ari F, Dimas K, Ikitimur EI, Guney E, Yilmaz VT (2011) Eur J Med Chem 46:4957–4963
28. Coskun MD, Ari F, Oral AY, Sarimahmut M, Kutlu HM, Yilmaz VT, Ulukaya E (2013) Bioorg Med Chem 21:4698–4705
29. Ari F, Aztopal N, Icsel C, Yilmaz VT, Guney E, Buyukgungor O, Ulukaya E (2013) Bioorg Med Chem 21:6427–6434
30. Icsel C, Yilmaz VT (2013) DNA Cell Biol 32:165–172
31. Banti CN, Giannoulis AD, Kourkoumelis N, Owczarzak AM, Poyraz M, Kubicki M, Charalabopoulos K, Hadjikakou SK (2012) Metallomics 4:545–560
32. Banti CN, Hadjikakou SK (2013) Metallomics 5:569–596
33. Ng SW (1995) Z Kristallogr 210:206–209
34. Cavicchioli M, Leite CQF, Sato DN, Massabni AC (2007) Arch Pharm Chem Life Sci 340:538–542
35. Yesilel OZ, Kastas G, Darcan C, Ilker I, Pasaoglu H (2010) Inorg Chim Acta 363:1849–1858
36. Sheldrick GM (2008) Acta Crystallogr Sect A 64:112–122
37. Spek AL (2003) J Appl Crystallogr 36:7–13
38. Pyle AM, Rehmann JP, Meshoyrer R, Kumar CV, Turro NJ, Barton JK (1989) J Am Chem Soc 111:3051–3058
39. Stern O, Volmer M (1919) Z Phys 20:183–188
40. Lee M, Rhodes AL, Wyatt MD, Forrow S, Hartley JA (1993) Biochemistry 32:4237–4245
41. Bi S, Qiao C, Song D, Tian Y, Gao D, Sun Y, Zhang H (2006) Sens Actuators B 119:199–208
42. Clinical Laboratory Standards Institute (2003) Approved standard M7-A6. Methods for dilution antimicrobial susceptibility tests for bacteria that grow aerobically, 6th edn. Clinical Laboratory Standards Institute, Wayne
43. Geary WJ (1971) Coord Chem Rev 7:81–122
44. Effendy, Hanna JV, Marchetti F, Martini D, Pettinari C, Pettinari R, Skelton BW, White AH (2004) Inorg Chim Acta 357:1523–1537
45. Di Nicola C, Effendy, Fazaroh F, Pettinari C, Skelton BW, Somers N, White AH (2005) Inorg Chim Acta 358:720–734
46. Effendy, Di Nicola C, Nitiatmodjo M, Pettinari C, Skelton BW, White AH (2005) Inorg Chim Acta 358:735–747
47. Effendy, Di Nicola C, Pettinari C, Pizzabiocca A, Skelton BW, Somers N, White AH (2006) Inorg Chim Acta 359:64–80
48. Pettinari C, Ngoune J, Marinelli A, Skelton BW, White AH (2009) Inorg Chim Acta 362:3225–3230
49. Zhang L, Lu X-Q, Zhang Q, Chen C-L, Kang B-S (2005) Transit Metal Chem 30:76–81
50. Daasch LW, Smith DC (1951) Anal Chem 23:853–868
51. Corbridge DEC (1956) J Appl Chem 6:546–465
52. Westermark G, Person I (1998) Colloids Surf A 144:149–166
53. Meijboom R, Bowen RJ, Berners-Price SJ (2009) Coord Chem Rev 253:325–342
54. James SL (2009) Chem Soc Rev 38:1744–1758
55. Hamamci S, Yilmaz VT, Harrison WTA (2005) Z Naturforsch 60b:978–983
56. Hamamci S, Yilmaz VT, Harrison WTA, Thöne C (2005) Solid State Sci 7:423–429
57. Yilmaz VT, Hamamci S, Kazak C (2005) Z Anorg Allg Chem 631:1961–1965
58. Hamamci S, Yilmaz VT, Harrison WTA (2005) Struct Chem 16:379–383
59. Yilmaz VT, Hamamci S, Buyukgungor O (2006) Z Naturforsch 61b:189–193
60. Yilmaz VT, Hamamci S, Gumus S, Buyukgungor O (2006) J Mol Struct 794:142–147
61. Gumus S, Hamamci S, Yilmaz VT, Kazak C (2007) J Mol Struct 828:181–187
62. Yilmaz VT, Senel E, Guney E, Kazak C (2008) Inorg Chem Commun 11:1330–1333
63. Hamamci S, Yilmaz VT, Gumus S, Buyukgungor O (2008) Struct Chem 19:123–129
64. Guney E, Yilmaz VT, Buyukgungor O (2010) Polyhedron 29:1437–1442
65. Ilker I, Yesilel OZ, Gunay G, Buyukgungor O (2009) J Organomet Chem 694:4178–4184
66. Yesilel OZ, Gunay G, Buyukgungor O (2011) Polyhedron 30:364–371

67. Szlyk E, Szymanska I, Surdykowski A, Glowiak T, Wojtezak A, Golinski A (2003) Dalton Trans 3404–3410
68. Lobbia GG, Pellei M, Pettinari C, Santini C, Skelton BW, White AH (2005) Polyhedron 24:181–187
69. Di Nicola C, Effendy, Pettinari C, Skelton BW, Somers N, White AH (2006) Inorg Chim Acta 359: 53–63
70. Effendy, Marchetti F, Pettinari C, Pettinari R, Skelton BW, White AH (2007) Inorg Chim Acta 360:1388–1413
71. Effendy, Marchetti F, Pettinari C, Pettinari R, Skelton BW, White AH (2007) Inorg Chim Acta 360:1414–1423
72. Teo P, Koh LL, Hor TSA (2008) Inorg Chem 47:9561–9568
73. Liu Y-L, Han L-J, Qiao G-R, Yang M, Zhang Q, Wang J-G, Zhan S-Z (2012) Synth React Inorg Met Org Nano Met Chem 42:183–189
74. Ruan B, Tian Y, Zhou H, Wu J, Liu Z, Zhu C, Yang J, Zhu H (2009) J Organomet Chem 694:2883–2887
75. Wang C-F, Peng S-M (1996) Polyhedron 15:1853–1858
76. Jones PG, Ahrens B (1998) Chem Commun 2307–2308
77. Su W, Hong M, Cao R, Chen J, Wu D, Liu H, Lu J (1998) Inorg Chim Acta 267:313–317
78. Lobana TS, Paul S, Castineiras A (1999) J Chem Soc Dalton Trans 1819–1824
79. Liu CW, Liaw B-J (2000) Inorg Chem 39:1329–1332
80. Youm K-T, Kim Y, Do Y, Jun M-J (2000) Inorg Chim Acta 310:203–209
81. Zhou W-B, Dong Z-C, Song J-L, Zeng H-Y, Cao R, Guo G-C, Huang J-S, Li J (2002) J Clust Sci 13:119–136
82. Park YJ, Do Y, Kim KM, Choi M-G, Jun M-J, Kim C (2002) Polyhedron 21:33–37
83. Zhang L, Zhang H-X, Chen C-L, Deng L-R, Kang B-S (2003) Inorg Chim Acta 355:49–56
84. Fournier E, Lebrun F, Drouin M, Decken A, Harvey PD (2004) Inorg Chem 43:3127–3135
85. Liu B, Zhou G-W, Fu M-L, Xu L, Guo G-C, Huang J-S (2004) Bull Korean Chem Soc 25:1937–1940
86. Di Nicola C, Ngoune J, Effendy, Pettinari C, Skelton BW, White AH (2007) Inorg Chim Acta 360:2935–2943
87. Ma Z, Sun J, Liu B, Hua M, Xing Y (2008) Acta Crystallogr Sect E 64:m269
88. Lo KM, Ng SW (2008) Acta Crystallogr Sect E 64:m717
89. Maa Z, Xing Y, Yang M, Hua M, Liu B, Guedes da Silva MFC, Pombeiro AJL (2009) Inorg Chim Acta 362:2921–2926
90. Lv Q-Y, Song Y-Q, Zhan S-Z, Cai J, He J-P (2009) J Coord Chem 62:1536–1543
91. Liu CW, Sarkar B, Liaw B-J, Lin Y-W, Lobana TS, Wang J-C (2009) J Organomet Chem 694:2134–2141
92. Song L-L, Cui L-N, Jina Q-H, Zhangb C-L (2010) Acta Crystallogr Sect E 66:m1237–m1238
93. Jin Q-H, Song L-L, Hu K-Y, Zhou L-L, Zhang Y-Y, Wang R (2010) Inorg Chem Commun 13:62–65
94. Song L-L, Jin Q-H, Cui L-N, Zhang C-L (2010) Inorg Chim Acta 363:2425–2429
95. Chao H-Y, Wu L, Li C-L, Lu W, Liu L, Feng X-L (2011) Z Anorg Allg Chem 637:1533–1538
96. Yang X, Huang X, Qiu Q-M, Jina Q-H, Zhang C-L (2012) Acta Crystallogr Sect E 68:m1367
97. Yilmaz VT, Hamamci S, Thöne C (2004) Z Anorg Allg Chem 630:1641–1644
98. Yilmaz VT, Hamamci S, Harrison WTA, Thöne C (2005) Polyhedron 24:693–699
99. Yilmaz VT, Hamamci S, Buyukgungor O (2008) Polyhedron 27:1761–1766
100. Prajapati R, Kimura K, Mishra L (2009) Inorg Chim Acta 362:3219–3224
101. Fournier E, Sicard S, Decken A, Harvey PD (2004) Inorg Chem 43:1491–1501
102. Aslanidis P, Cox PJ, Divanidis S, Karagiannidis P (2004) Inorg Chim Acta 357:2677–2686
103. Bao F, Lu X-Q, Ng SW (2005) Acta Crystallogr Sect E 61:m2637–m2638
104. Zhang L, Lu X-Q, Chen C-L, Tan H-Y, Zhang H-X, Kang B-S (2005) Cryst Growth Des 5:283–287
105. Cingolani A, Effendy, Pettinari C, Skelton BW, White AH (2006) Inorg Chim Acta 359:2170–2177
106. De Menezes Vicenti JR, Burrow RA (2007) Acta Crystallogr Sect C 63:m88–m90
107. Wang X-C, Wu Y-L, You X-L (2008) Acta Crystallogr Sect E 64:m981
108. Teo YY, Lo KM, Ng SW (2008) Acta Crystallogr Sect E 64:m819
109. Dennehy M, Quinzani OV, Mandolesi SD, Burrow RA (2011) J Mol Struct 998:119–125
110. Ruina Y, Yimin H, Baoyu X, Dungmei W, Douman J (1996) J Trans Met Chem 21:28–30
111. Cui L-N, Li Z-F, Jin Q-H, Xin X-L, Zhang C-L (2012) Inorg Chem Commun 20:126–130
112. Zhang L, Chen C, Zhang Q, Zhang H, Kang B (2003) Acta Crystallogr Sect E 59:m536–m537
113. Lepecq J-B, Paoletti C (1967) J Mol Biol 27:87–106
114. Richards AD, Rodger A (2007) Chem Soc Rev 36:471–483
115. Nomiya K, Kondoh Y, Onoue K, Kasuga NC, Nagano H, Oda M, Sudoh T, Sakuma S (1995) J Inorg Biochem 58:255–267
116. Noguchi R, Sugie A, Okamoto Y, Hara A, Nomiya K (2005) Bull Chem Soc Jpn 78:1953–1962
117. Berners-Price SJ, Johnson RK, Giovenella AJ, Faucette LF, Mirabelli CK, Sadler PJ (1988) J Inorg Biochem 33:285–295